IEEE Robotics and Automation Letters (RAL) paper presented at the
2020 IEEE/RSJ International Conference on Intelligent Robots and Systems (IROS)
October 25-29, 2020, Las Vegas, NV, USA (Virtual)

Compliant Control and Compensation for A Compact Cable-driven Robotic Manipulator*

Jing Li[1], James Lam[1], and Zheng Wang[1,2]

Abstract— **Cable-driven robotic manipulators are desirable for medical applications, for their form factor flexibility after separating actuation from the distal end. However, intended to work under high spatial constraints such as dental or other surgical applications, severe cable elongations will raise control challenges from inaccuracy to excessive compliance. It is critical to proactively regulate the system compliance, in order to achieve both compliant behavior to avoid tissue damage, and rigid behavior necessary for dental drilling. Both ends of this challenges have been extensively studied in literature, with rigidity achieved by cable elongation compensation, and virtual compliance regulation by impedance control. However, each approach worked within its own turf, with very little being studied in how to blend the two sources of compliance strategically. In this work, blending virtual compliance modulated by impedance control with transmission compliance induced by cable elasticity was investigated and demonstrated in a modified design of our proprietary dental manipulator. It was shown that direct application of impedance control in a cable-driven system would not bluntly increase compliance, and may cause instability. Instead, we proposed a compliance-blending framework with Cartesian-space super-positioning of cable motion compensation and impedance control, and validated the efficacy on the 6-DOF dental manipulator platform. Desirable results were achieved using highly common approaches in both impedance control and cable compensation, making the proposed approach applicable to a wide range of cable-driven robotic systems for impedance control.**

I. INTRODUCTION

Oral diseases are common in the general public [1], but could deteriorate severely without timely treatments [2], [3], largely due to the global shortage of dentists [4]. This calls for robotic solutions to migrate their previous success in assisting surgeries [5] to dental treatments [6]. Existing dental robots based on industrial manipulators [7], [8], had workspaces excessive for the human oral cavity for the footprint and cost. In our previous works, we designed a dental-specific compact manipulator with fitting workspace [9]–[11]. Cable transmission (aka tendon-sheath transmission) was employed to separate actuation from the manipulator for reduced weight and compactness [10], with teleoperation and motion scaling being implemented [11]. However, transmission inaccuracy due to cable elasticity under loading was

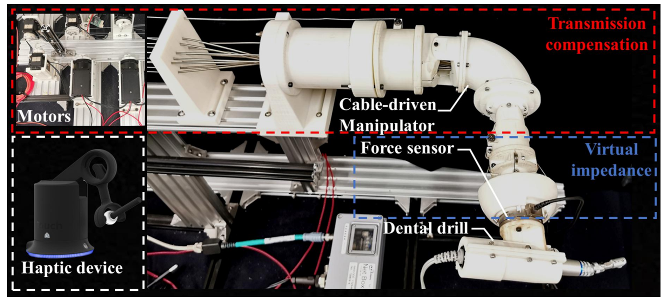

Fig. 1. The proposed robotic system.

not considered, as the previous works were mainly involving free-space motions.

In this work, we extend the investigation to force interactions for tasks such as dental drilling, while position accuracy could not be compromised. This calls for an elevated level of compliance regulation, on top of the inherent mechanical compliance from the cable transmission itself.

For cable-driven transmission systems, cable elongation is often ignored when applying computed compliant control [12], [13]. Cable elongation issues are considered in literature mainly to eliminate its effect towards better positioning accuracy, with compensation methods proposed using different offline [14]–[20] and online [21] friction models, as well as using learning-based approaches [22]. They were targeted at reducing or eliminating cable compliance, rather than introducing other sources of compliance artificially (such as impedance control), to proactively controlling the overall system compliance. On the other hand, compliance regulation has been extensively studied for rigid robots by impedance control [23]–[26] or admittance control [27] for different manipulator types (both referred to as "impedance control" for brevity in the limited context of this paper), without considering transmission compliance.

There is little study in the literature, regarding how to blend the virtual compliance from impedance control with the physical compliance from cable transmission, with non-negligible cable elongation. This is particularly relevant to compact cable-driven robot designs with large cable length-diameter ratios for medical applications.

In this work, compliance blending and regulation was investigated for cable-driven robotic systems. After presenting a bottom-up redesign of our proprietary dental manipulator for various performance improvements, we presented investigations conducted on the updated manipulator platform. Using well-acknowledged approaches for both impedance

*The presented research has been supported by Hong Kong ITF Grant ITS/140/18 & ITS457/17FP & ITS/305/19FP & NSFC General Grant 51975268 & AISONO-SUSTech Joint Lab Fund & SZ/HK Innov. Circle Type-D SGDX20190816232011196.

[1]J. Li, J. Lam and Z. Wang are with the Department of Mechanical Engineering, the University of Hong Kong, Hong Kong SAR, China lijingtsinghua11@gmail.com; jlam@hku.hk

[2]Z. Wang is also with the Department of Mechanical and Energy Engineering, Southern University of Science and Technology, China. wangz@sustech.edu.cn

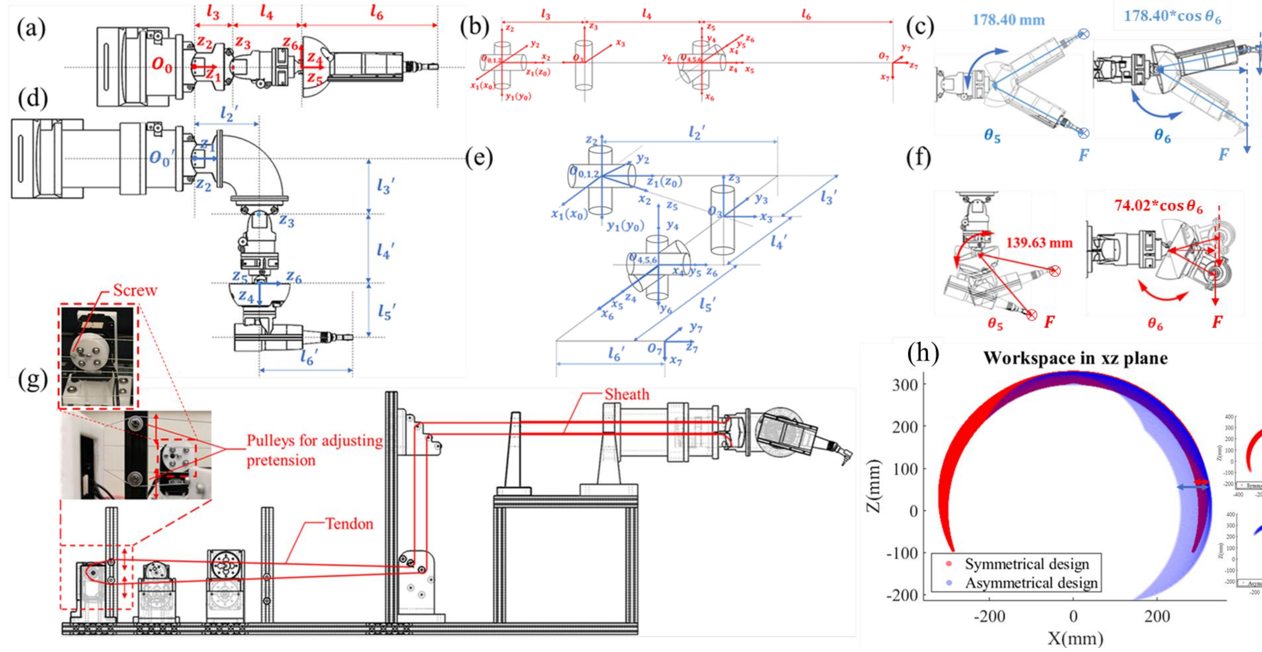

Fig. 2. The proposed robotic manipulator. (a) Symmetrical configuration. (b) Kinematics model of symmetrical configuration. (c) Rotating arm of joint 5 and joint 6 of symmetrical configuration. (d) Asymmetrical configuration. (e) Kinematics model of asymmetrical configuration. (f) Rotating arm of joint 5 and joint 6 of asymmetrical configuration. (g) Tendon-sheath mechanism of an asymmetrical configuration. (h) Workspace on XZ plane of two configurations.

TABLE I
SYSTEM PARAMETERS

Symmetrical dimension (mm)		Asymmetrical dimension (mm)	
l_3	53.50	l_2'	90.50
l_4	97.80	l_3'	77.50
l_6	178.40	l_4'	97.50
		l_5'	74.02
		l_6'	118.39

control and cable motion compensation, we proposed a compliance blending framework with Cartesian space algebraic super-positioning, for cable-driven systems. The overall concept and system components will be introduced in Section II; the manipulator design modifications with a new asymmetrical configuration will be described and compared against our previous design in Section III; where Section IV will focus on compliance regulation based on cable motion compensation and impedance control, where a novel compliance blending framework on Cartesian-space super-positioning will be proposed, validated by experimental results in Section V.

II. SYSTEM INTEGRATION

Our robotic system is composed of a six-DOF manipulator, with a force sensor attached to the wrist joint, six motors for actuation, cables covered by sheath for motion and force transmission, and a haptic device for input signal generations as shown in Fig. 1.

The proposed robotic manipulator is controlled in a master-slave manner, the master side of which is mainly responsible of input signal generation as well as transformation from master to slave including motion scaling and coordinate transformation, while the slave system contains both actuation part and the manipulator itself. The actuation part is composed of six motors (DYNAMIXEL), one for each joint. A force sensor (ATI mini45) was installed to measure the force and torque of the wrist joint in real time.

The overall control algorithm was programmed on SIMULINK (Matlab 2019a, MathWorks). The communications between SIMULINK and hardware as motors, haptic device and force sensor were realized via UDP.

III. SYSTEM DESIGN AND ANALYSIS

A. Asymmetrical Configuration

The proposed robotic manipulator is composed of six joints, including two cylindrical joints, two revolute joints and one wrist joint with two joints' axes perpendicularly with each other, formed by a universal joint. The rotational axes of last three joints intersect with each other to one point which enables decomposing of position and orientation and closed-form solutions in inverse kinematics analysis can therefore be obtained. Different from our previous symmetrical design as shown in Fig. 2 (a) [10], an asymmetrical design was applied, by inserting the 'L'-shaped part between the second and third joint as shown in Fig. 2 (d).

This modification has advantages as enlarging the workspace on XZ plane and avoiding certain singularity pose compared with the symmetrical design. As shown in Fig. 2 (h), the workspace on XZ plane was plotted with only the second and third joints of each configuration rotating within their joint limits, where the blue points represent the

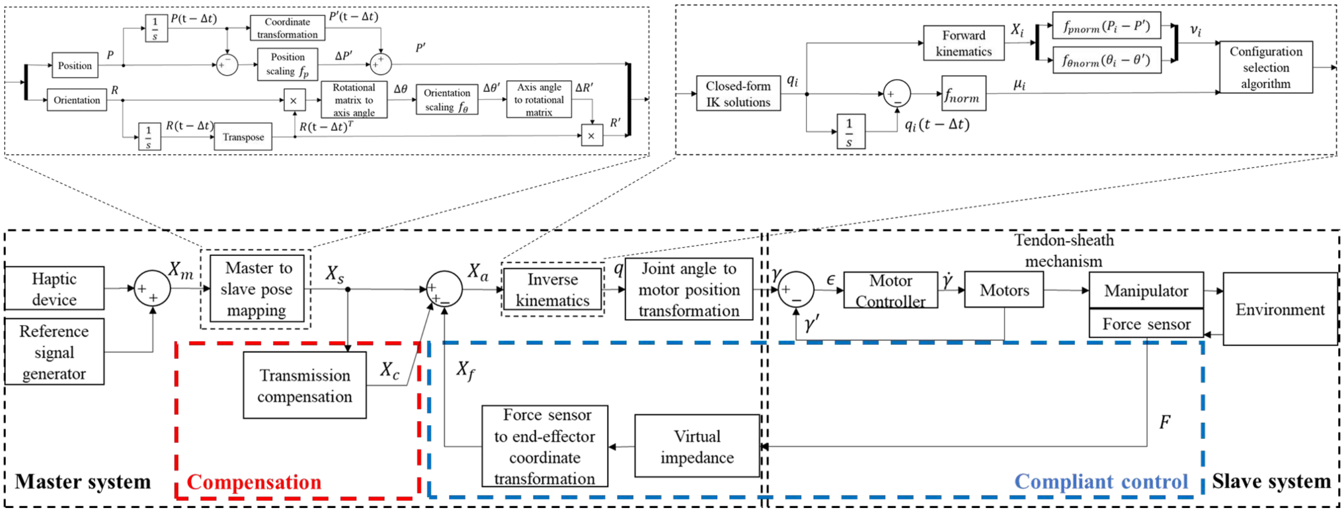

Fig. 3. Control diagram of the proposed robotic system. X_m represents the combined input signals, X_s represents the target position and orientation for slave system. X_c represents the displacement compensation, and X_f is the displacement computed by impedance model and force feedback F with coordinate transformation. X_a is the actuated trajectory by integration of X_s, X_c and X_f. Joint angles are q after inverse kinematics analysis, and γ represents goal positions of motors, γ' is the real positions read from motor encoders, and ϵ is the error between them. $\dot{\gamma}$ is the velocity set to motors. In master-slave mapping algorithm, P represents the position and R represents the rotational matrix. P' is the position processed with coordinate transformation and incrementation of scaled position differences $\Delta P'$, and R' is the rotational matrix after multiplying with scaled orientation changes $\Delta R'$. In inverse kinematics analysis, q_i is the i^{th} solution of joint angles, and X_i is the corresponding motion calculated by Forward kinematics. μ_i and ν_i are normalized joint angle difference and motion difference for i^{th} solution.

reachable points of asymmetrical structure, and red points are the reachable points for symmetrical structure. And it is clearly shown that the asymmetrical structure has larger motion range than the symmetrical one. Additionally, the symmetrical structure has a singularity position as shown in Fig. 2 (a), with the arm stretching out and reaching its workspace boundary. To avoid such pose, the starting pose need to be carefully chosen and the motion range would be limited to only one side of its workspace.

The modified asymmetrical structure on the other hand could avoid such singularity pose naturally which is beneficial to real applications, since the pose shown in Fig. 2 (d) could work directly as a clinical configuration with a larger motion range as similar in [28]. Instead of installing the dental drill along the rotational axis of the whole arm as shown in Fig. 2 (a), we installed the dental drill perpendicularly in order to shorten the distance between the end of dental drill and the center of the last joint. As presented in Fig. 2 (c) and (f), the rotating arms of joint 5 and joint 6 of asymmetrical design are smaller than the symmetrical design and the torque of the last two joints of the same load would be reduced as well.

B. Kinematics Analysis

Transformation matrices between neighboring frames can be written based on geometrical relation in between as shown in Fig. 2 (e). Assuming that the origin of the proposed manipulator base frame is located at (x_0, y_0, z_0), the origin of the last joint frame O_6 is located at (x_6, y_6, z_6), the joint angle of i^{th} joint is θ_i. And the position of the last joint origin can be expressed as:

$$x_6 = c\theta_1(l_4 c\theta_{2+3} + l_3 c\theta_2 - l_2 s\theta_2) \tag{1}$$

$$y_6 = s\theta_1(l_4 c\theta_{2+3} + l_3 c\theta_2 - l_2 s\theta_2) \tag{2}$$

$$z_6 = l_4 s\theta_{2+3} + l_3 s\theta_2 + l_2 c\theta_2 + l_0 \tag{3}$$

The inverse kinematics can be calculated as:

$$\theta_1 = 2\arctan\frac{-x_6 \pm \sqrt{{x_6}^2 + {y_6}^2}}{y_6} \tag{4}$$

$$\theta_2 = 2\arctan\frac{t \pm \sqrt{t^2 - (z_6' + l_4 s\theta_3 + l_2)(z_6' - l_4 s\theta_3 - l_2)}}{z_6' + l_4 s\theta_3 + l_2} \tag{5}$$

$$\theta_3 = 2\arctan\frac{2l_2 l_4 \pm \sqrt{4{l_2}^2{l_4}^2 - (r^2 + 2l_3 l_4)(r^2 - 2l_3 l_4)}}{r^2 + 2l_3 l_4} \tag{6}$$

Where ${z_6}' = z_6 - l_0$, $s\theta = sin\theta$, $c\theta = cos\theta$, $r^2 = {x_6}^2 + {y_6}^2 + {z_6'}^2 - {l_2}^2 - {l_3}^2 - {l_4}^2$, $t = l_4 cos\theta_3 + l_3$. The last three joints can be computed from rotational transformation matrix ${}^3_6R$ according to rotational matrices relation ${}^3_6R$=${}^0_3R^T\,{}^0_6R$. All the dimensions mentioned here are listed in Table I.

C. Tendon-sheath Transmission Mechanism

The tendon-sheath mechanism of our current manipulator remains the same as our previous one for their superior capability of transmitting force and motion under flexible constrained path [10]. Each joint is connected with one motor by a pair of tendons, for two rotational directions. A supporting part was installed on each motor, which the tendons are fixed to by screws. Pretension was added and adjusted by changing two opposing pulley positions as shown in Fig. 2 (g) and we increase pretension by enlarging the distance between two pulleys, while decreasing it by moving two pulleys closer. Each joint is coupled with two pulleys, each pulley for one cable. We kept each pulley at the same

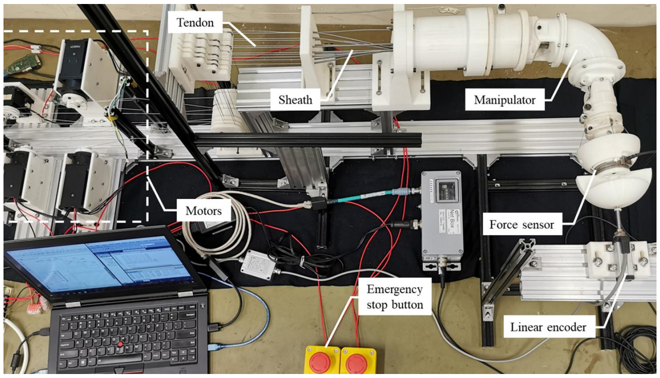

Fig. 4. Experimental setup.

TABLE II
COMPENSATION COEFFICIENTS

Coefficients k_i	Sine wave with amplitude as 5mm	Sine wave with amplitude as 6mm
k_1	1.90	1.75
k_2	1.20	1.20
k_3	1.30	1.25
k_4	0.60	0.60

position for each test to keep pretension the same for all the tests.

IV. COMPLIANT CONTROL AND COMPENSATION

Overall system control of our previous symmetrical design was elaborated in [10], [11], including teleoperation implementation, mapping from master to slave, inverse kinematics solutions selection, as well as motor control as shown in Fig. 3. Our system is controlled in a master-slave manner, where the haptic device works as the master system, controlled by dentists and generating input signals X_m. The input signals will be transformed and scaled down firstly to generate the target motions of slave system X_s, which will be used to calculate joint angles q by inverse kinematics analysis and be further transformed to motors goal positions γ. The velocity commands $\dot{\gamma}$ for controlling motors will be generated by comparing the desired and real motor positions. The manipulator will then be actuated by motors via tendon-sheath mechanism as mentioned before. Current control algorithm was built based the previous version, where inverse kinematics analysis was changed due to the configuration modulation, and reference signal generator was added in order to test with standard signals such as sine wave, square wave, zigzag wave etc. Apart from these adjustments, impedance control and compensation component were added as well, highlighted with dashed blue and red block respectively shown in Fig. 3.

A. Compensation for Cable Elongation and Hysteresis

Inspired by [20], compensation aiming at decreasing motion tracking error caused by cable elongation and hysteresis was implemented by feed-forwarding a displacement to the actuator, which can be described as:

$$X_a = X_s + X_c \tag{7}$$

The compensation displacement for cable elongation is computed by multiplying desired trajectory with a coefficient. The coefficient was chosen based on experimental results and varies under different peak values of desired trajectories, while remaining the same for the desired trajectory with different frequencies but the same peak value.

In our case, a linear encoder is always in touch with the manipulator end-effector to measure its displacement. The spring of linear encoder for position restoration generated force opposing manipulator's moving direction. Larger the manipulator displacement is, larger the opposing force becomes, and so will the cable elongation be. Therefore, coefficients for compensation differ for different motion directions.

To further compensate for backlash hysteresis, we speed up the acceleration process of motors commutation, where the hysteresis usually happen due to the delay between motor commutation and corresponding cable tightening. By challenging the motor to turn at its highest speed, the delay in between can be shortened, and the error caused by hysteresis should be reduced. The relation between desired trajectories and compensation for both cable elongation and hysteresis can be described as:

$$X_c = \begin{cases} k_1 X_s, & X_s \geq 0 \quad \&\& \quad X_s(t) - X_s(t-\Delta t) \geq 0, \\ k_2 X_s, & X_s < 0 \quad \&\& \quad X_s(t) - X_s(t-\Delta t) < 0, \\ k_3 X_s, & X_s \geq 0 \quad \&\& \quad X_s(t) - X_s(t-\Delta t) < 0, \\ k_4 X_s, & X_s < 0 \quad \&\& \quad X_s(t) - X_s(t-\Delta t) \geq 0. \end{cases} \tag{8}$$

Where k_i, $i = 1, 2, 3, 4$, represents different coefficients under different conditions and their specific values for different amplitudes were listed in Table II. And the zero position of X_s corresponds to the critical point when the end-effector starts to contact with the environment.

B. Compliance Modulation with Impedance Control

Apart from inherent compliance of cable-driven manipulators, virtual compliance has also been considered and modulated in our control algorithm. Inspired by [23]–[25], a second order impedance model was applied in regulating force and position relation in Cartesian space as shown in Fig. 3 within dashed blue block. The impedance model can be expressed as:

$$M(\ddot{X} - \ddot{X}_d) + D(\dot{X} - \dot{X}_d) + K(X - X_d) = F \tag{9}$$

Where M, D, K represent mass, damping and stiffness coefficients respectively, X_d is the virtual reference trajectory, F is the measured force and $\Delta X = X - X_d$ is the corresponding displacement. After coordinate transformation from force sensor to end-effector coordinates of ΔX, the displacement for end-effector X_f was directly integrated to the desired trajectory X_s as shown in Fig. 3 and can be expressed as:

$$X_a = X_s + X_c + X_f \tag{10}$$

By adjusting parameters M, D, K in impedance model, virtual compliance can be amended, and the manipulator

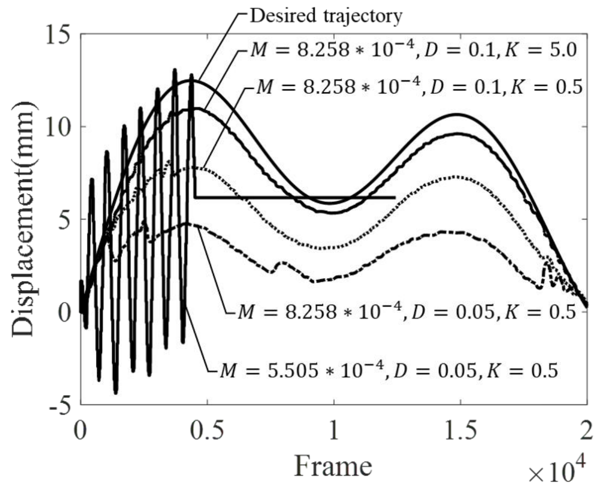

Fig. 5. Experimental results of preliminary impedance control tests with different impedance parameters.

could appear to be actively responding to the environment with different compliance, ranging from 'soft' to 'stiff'.

V. EXPERIMENTAL VALIDATION

The experimental setup is shown in Fig. 4. A linear encoder (KTR2-15mm) was installed for measuring end-effector displacement and is always in contact with the manipulator during tests. The linear encoder data was read from an Arduino Mega board and recorded by a serial port debugging software (ATK-XCOM v2.0). Data of motor positions, velocities, input signals were recorded by SIMULINK (Matlab 2019a, Mathworks) in real time. All the data was synchronized chronologically afterwards.

Preliminary tests of impedance control were performed without any compensation and the results are shown in Fig. 5. Instead of a linear encoder, we used an aluminum plate as the stiff obstacle and expected the manipulator to reach an equilibrium position right in front of it. However unreliable motion transmissions of uncompensated cable-driven mechanism made it almost impossible to achieve stable impedance control result. It also appeared extremely difficult and impractical to find appropriate impedance parameters for the system to balance under such circumstance. As shown in Fig. 5, there is not much adjustment space before the system gets unstable.

A. Motion Tracking Test

To validate motion tracking performance of our manipulator, a sine wave of 5 mm amplitude and 0.5 rad/s frequency was generated as an input signal and is shown in Fig. 6 (a), where the black line represents the desired sine wave trajectory, blue line represents the actuated trajectory, and red line represents the linear encoder measurement. Actuators' commands are the same as the desired sine wave therefore the black line is overlapped with the blue line.

Cable elongation and system hysteresis were revealed in motion tracking result in Fig. 6 (a). Opposing force generated by the linear encoder was also displayed in the asymmetrical red line. The tendency of larger displacement causing larger cable elongation and larger tracking error can be inferred as well.

B. Motion Tracking Tests with Compensation

Experimental result of motion tracking with only cable elongation compensation is shown in Fig. 6 (b), and Fig. 6 (c) shows the result with compensation for cable elongation as well as hysteresis, where the same desired trajectory for all three tests was applied shown as black line and the compensated actuated trajectories are marked as blue. The red lines representing measured trajectories present less motion tracking error compared with Fig. 6 (a), where no compensation was implemented. To be specific, the tracking error has been reduced 75 %, from averaging 4.18 mm to 1 mm after applying compensation for cable elongation.

The relations between desired displacement and the manipulator end-effector displacement (measured by linear encoder displacement) for different cases are presented in Fig. 6 (d), where light blue line represents result without compensation, red line represents the one with only cable elongation compensation, and yellow line represents the result with compensation for both elongation and hysteresis.

Six phases can be distinguished for each test from Fig. 6 (d). For phase I, the input signal starts to increase, while the end-effector remains stable, which is mainly caused by insufficient pretension. In phase II, the end-effector starts to move forward and the relations between measured displacements of end-effector and the desired ones can be approximated as linear relations for all three cases. In phase III, the input signal starts to change directions, and actuates the end-effector to move backwards while it actually stays at the same position. In phase IV, the end-effector starts to move backwards and the relations between desired displacements and end-effector displacements appear to be linear as well. In phase V, the input signal changes its sign while the end-effector holds still. The last phase, phase VI shows similar relations as in phase II.

Asynchronization between desired and real trajectories in phase III and V are caused by system hysteresis and it is intuitive that larger the desired displacements are required for actuating the manipulator to start moving, larger the system hysteresis must be. Comparing phase III in three cases, the one with hysteresis compensation shows the smallest hysteresis, which confirms the positive effect of the modified actuated trajectory in the first half of each cycle. And the desired displacement needed for counteracting hysteresis has been reduced from 2.0449 mm to 0.2655 mm, with only 13 % left compared with the result without any compensation. However, the modified trajectory with similar logic in the second half of each cycle does not bring obvious improvements when comparing results in phase V, which should be induced by the opposing force when contacting with the linear encoder.

Fig. 6 (e) and (f) present the motion tracking results with compensation for both cable elongation and hysteresis of varied desired trajectories. The desired trajectory in Fig.

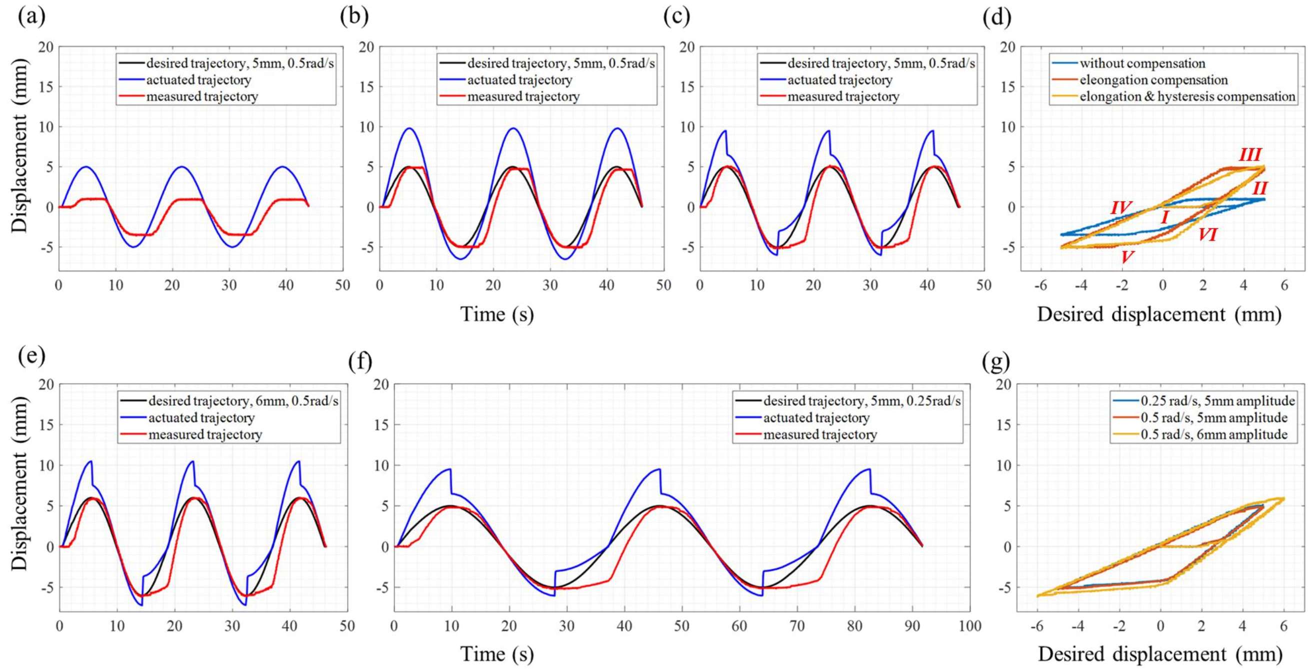

Fig. 6. Experimental results of motion tracking with and without compensation. (a) Motion tracking result without compensation, desired trajectory as sine wave, 5mm amplitude, 0.5 rad/s frequency. (b) Motion tracking result with compensation for cable elongation, desired trajectory as sine wave, 5mm amplitude, 0.5 rad/s frequency. (c) Motion tracking result with compensation for both cable elongation and hysteresis, desired trajectory as sine wave, 5mm amplitude, 0.5 rad/s frequency. (d) Measured displacements plot against desired displacements corresponding to motion tracking results in (a)-(c). (e) Motion tracking result with compensation for both cable elongation and hysteresis, desired trajectory as sine wave, 6mm amplitude, 0.5 rad/s frequency. (f) Motion tracking result with compensation for both cable elongation and hysteresis, desired trajectory as sine wave, 5mm amplitude, 0.25 rad/s frequency. (g) Measured displacements plot against desired displacements corresponding to motion tracking results in (c), (e)-(f).

6 (e) is a sine wave with 6 mm amplitude and 0.5 rad/s frequency while in Fig. 6 (f), the desired trajectory is a sine wave with 5mm amplitude and 0.25 rad/s frequency. Plot of measured displacements against desired displacements with different desired trajectories is shown in Fig. 6 (g), where all tests have been compensated for both cable elongation and hysteresis, corresponding to results presented in Fig. 6 (c), (e) and (f). In Fig. 6 (g), the light blue line corresponds to motion tracking of a sine wave with 5 mm amplitude and 0.25 rad/s frequency, and red line represents motion tracking of a sine wave with 5 mm amplitude and 0.5 rad/s frequency, while yellow line shows motion tracking of a sine wave with 6 mm amplitude and 0.5 rad/s frequency. The compensation coefficients for desired trajectories with the same amplitude were the same and decreased a little for the one with larger amplitude.

C. Position-based Impedance Control with Compensation

Virtual compliance was modulated by applying impedance model and adjusting its parameters. The actuated trajectory was computed by summing up the desired signals, the corresponding compensation and the displacements calculated by impedance model as (9). Corresponding results are presented in Fig. 7.

In Fig. 7 (a)-(c), results of tracking the same desired trajectory with different impedance parameters are presented, where the mass coefficients are equal to the manipulator mass as 0.0008258, and the damping and stiffness coefficients differed as $(D = 1, K = 1)$, $(D = 0.1, K = 1)$ and $(D = 0.05, K = 0.5)$ respectively. However, there is a boundary for amending impedance parameters and once the impedance model is 'too compliant', the system will become unstable as shown in Fig. 7 (d), where the impedance parameters are $M = 0.0008258, D = 0.1, K = 0.1$.

Fig. 7 (e) presents the relations between the desired displacement and measured displacement of all three tests with different impedance parameters as mentioned above and labeled in the figure as well as the test without impedance control. Similar to Fig. 6 (d), there are six phases and the efficacy of compensation can also be evaluated from phase III for all three tests. For phase II and phase VI, the relations between desired and measured displacements can be estimated with linear relations and the slope of each test varies from maximum 1.9302 for test without impedance control to minimum 0.7865 for the one with the most compliant parameters. While the slopes of the remaining two tests with stiffness coefficient $K = 1$ are 1.5233 and 1.4319 respectively, nearly twice compared to the one with $K = 0.5$.

To evaluate the system compliance, applied force against the corresponding displacement was plotted in Fig. 7 (f) and the corresponding displacement was computed by subtracting the linear encoder measurements from the desired trajectory. In addition to remaining hysteresis, displacement-to-force ratios of different tests can be distinguished and considered

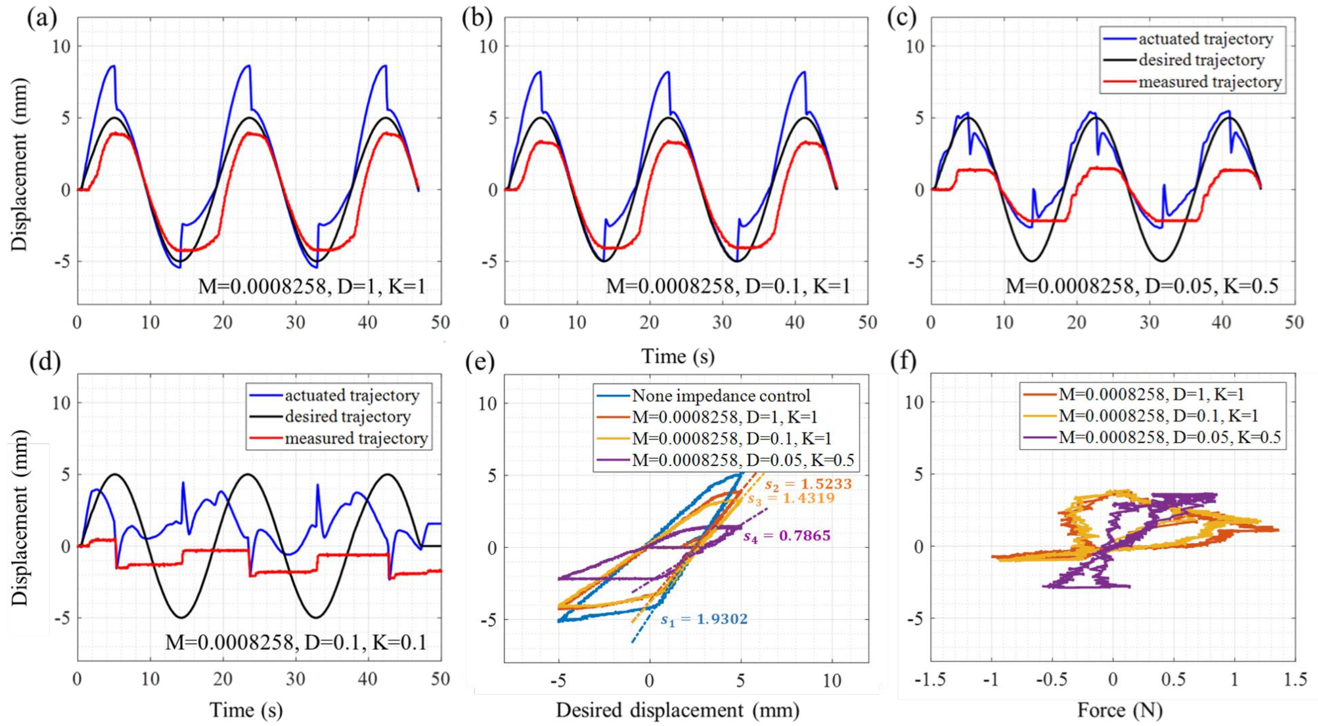

Fig. 7. Experimental results of compliant control with compensation. (a)-(d) Impedance control with compensation with different parameters, (a) $M = 0.0008258, D = 1, K = 1$ (b) $M = 0.0008258, D = 0.1, K = 1$ (c) $M = 0.0008258, D = 0.05, K = 0.5$, (d) $M = 0.0008258, D = 0.1, K = 0.1$ (e) Measured displacement plot against desired displacement of different parameters corresponding to compliant control results in (a)-(c). (f) Displacement differences between desired and measured trajectories against applied force under different conditions corresponding to compliant control results in (a)-(c).

as the system compliance. Larger the displacement-to-force ratio is, more compliant the system appears. The yellow line representing the test with the 'softest' impedance parameters also shows the largest system compliance as desired.

VI. CONCLUSION AND FUTURE PLAN

In this paper, blending virtual compliance from impedance control with the physical compliance resulting from transmission cable elasticity was investigated. And our results have revealed: 1) Impedance control will not simply make a cable-driven system more compliant compared with its physical compliance induced by cables, which is quite different from rigid robots. And too aggressive impedance parameters may cause instability of the system. 2) Motion compensation was proved to be an effective remedy for implementing impedance control in cable transmission systems. However, the practical range of compliance regulation for impedance control is limited within the range of "added" rigidity resulting from the motion compensation. This is somewhat a "zero-sum" situation, regarding the overall compliance of the system. 3) Our experimental results also validated the feasibility of applying impedance control in cable-driven system in end-effector Cartesian space, despite the multi-DOF nature of the manipulator. With the well-acknowledged approaches we used for both impedance control and motion compensation and the straightforward Cartesian space algebraic super-positioning as well as the development of miniature force sensors [29], the proposed framework will be applicable in a wider range of cable-driven robotic systems to enable compliance regulation and control.

In the future, the effect of asymmetrical structure on our compliant control and compensation will be investigated and compensation in joint level will be considered. A more specific model in analyzing the relation between the virtual and inherent compliance could be further studied and may play an important role in control of cable-driven mechanism in the future.

REFERENCES

[1] T. Vos, A. A. Abajobir, K. H. Abate, C. Abbafati, K. M. Abbas, F. Abd-Allah, R. S. Abdulkader, A. M. Abdulle, T. A. Abebo, S. F. Abera *et al.*, "Global, regional, and national incidence, prevalence, and years lived with disability for 328 diseases and injuries for 195 countries, 1990–2016: a systematic analysis for the global burden of disease study 2016," *The Lancet*, vol. 390, no. 10100, pp. 1211–1259, 2017.

[2] F. Bray, J. Ferlay, I. Soerjomataram, R. L. Siegel, L. A. Torre, and A. Jemal, "Global cancer statistics 2018: Globocan estimates of incidence and mortality worldwide for 36 cancers in 185 countries," *CA: a cancer journal for clinicians*, vol. 68, no. 6, pp. 394–424, 2018.

[3] G. W. Taylor and W. Borgnakke, "Periodontal disease: associations with diabetes, glycemic control and complications," *Oral diseases*, vol. 14, no. 3, pp. 191–203, 2008.

[4] "Health facts of hong kong," https://www.dh.gov.hk/english/statistics/statistics_hs/files/Health_Statistics_pamphlet_E.pdf.

[5] M. Gómez Ruiz, S. Alfieri, T. Becker, M. Bergmann, U. Boggi, J. Collins, N. Figueiredo, I. Gögenur, K. Matzel, D. Miskovic *et al.*, "Expert consensus on a train-the-trainer curriculum for robotic colorectal surgery," *Colorectal Disease*, vol. 21, no. 8, pp. 903–908, 2019.

[6] P. Gomes, "Surgical robotics: Reviewing the past, analysing the present, imagining the future," *Robotics and Computer-Integrated Manufacturing*, vol. 27, no. 2, pp. 261–266, 2011.

[7] M. Rawtiya, K. Verma, P. Sethi, and K. Loomba, "Application of robotics in dentistry," *Indian J Dent Adv*, vol. 6, no. 4, pp. 1700–1706, 2014.

[8] Z. Haidar, "Autonomous robotics: A fresh era of implant dentistry... is a reality!" *Journal of Oral Research*, vol. 6, no. 9, pp. 230–231, 2019.

[9] J. Li, W. Y. H. Lam, R. T. C. Hsung, E. H. N. Pow, and Z. Wang, "A customizable, compact robotic manipulator for assisting multiple dental procedures," in *2018 3rd International Conference on Advanced Robotics and Mechatronics (ICARM)*. IEEE, 2018, pp. 720–725.

[10] J. Li, Z. Shen, W. Y. T. Xu, W. Y. H. Lam, R. T. C. Hsung, E. H. N. Pow, K. Kosuge, and Z. Wang, "A compact dental robotic system using soft bracing technique," *IEEE Robotics and Automation Letters*, vol. 4, no. 2, pp. 1271–1278, 2019.

[11] J. Li, W. Y. H. Lam, R. T. C. Hsung, E. H. N. Pow, C. Wu, and Z. Wang, "Control and motion scaling of a compact cable-driven dental robotic manipulator," in *2019 IEEE/ASME International Conference on Advanced Intelligent Mechatronics (AIM)*. IEEE, 2019, pp. 1002–1007.

[12] K. Haninger, J. Lu, and M. Tomizuka, "Robust impedance control with applications to a series-elastic actuated system," in *2016 IEEE/RSJ International Conference on Intelligent Robots and Systems (IROS)*, 2016, pp. 5367–5372.

[13] W. M. dos Santos and A. A. Siqueira, "Impedance control of a rotary series elastic actuator for knee rehabilitation," *IFAC Proceedings Volumes*, vol. 47, no. 3, pp. 4801 – 4806, 2014, 19th IFAC World Congress. [Online]. Available: http://www.sciencedirect.com/science/article/pii/S1474667016423578

[14] S. J. Phee, S. Low, P. Dario, and A. Menciassi, "Tendon sheath analysis for estimation of distal end force and elongation for sensorless distal end," *Robotica*, vol. 28, no. 7, pp. 1073–1082, 2010.

[15] Z. Sun, Z. Wang, and S. J. Phee, "Elongation modeling and compensation for the flexible tendon–sheath system," *IEEE/ASME Transactions on Mechatronics*, vol. 19, no. 4, pp. 1243–1250, 2013.

[16] W. Xu, C. C. Poon, Y. Yam, and P. Chiu, "Motion compensated controller for a tendon-sheath-driven flexible endoscopic robot," *The International Journal of Medical Robotics and Computer Assisted Surgery*, vol. 13, no. 1, p. e1747, 2017.

[17] G. Palli, G. Borghesan, and C. Melchiorri, "Modeling, identification, and control of tendon-based actuation systems," *IEEE Transactions on Robotics*, vol. 28, no. 2, pp. 277–290, 2011.

[18] Q. Wu, X. Wang, L. Chen, and F. Du, "Transmission model and compensation control of double-tendon-sheath actuation system," *IEEE Transactions on Industrial Electronics*, vol. 62, no. 3, pp. 1599–1609, 2014.

[19] Z. Shao, Q. Wu, B. Chen, H. Wu, and Y. Zhang, "Modeling and inverse control of a compliant single-tendon-sheath artificial tendon actuator with bending angle compensation," *Mechatronics*, vol. 63, p. 102262, 2019.

[20] Z. Sun, Z. Wang, and S. J. Phee, "Modeling and motion compensation of a bidirectional tendon-sheath actuated system for robotic endoscopic surgery," *Computer methods and programs in biomedicine*, vol. 119, no. 2, pp. 77–87, 2015.

[21] T. N. Do, T. Tjahjowidodo, M. W. S. Lau, and S. J. Phee, "Position control of asymmetric nonlinearities for a cable-conduit mechanism," *IEEE Transactions on Automation Science and Engineering*, vol. 14, no. 3, pp. 1515–1523, 2015.

[22] X. Li, L. Cao, A. M. H. Tiong, P. T. Phan, and S. J. Phee, "Distal-end force prediction of tendon-sheath mechanisms for flexible endoscopic surgical robots using deep learning," *Mechanism and Machine Theory*, vol. 134, pp. 323–337, 2019.

[23] N. Hogan, "Impedance control: An approach to manipulation," in *1984 American control conference*. IEEE, 1984, pp. 304–313.

[24] ——, "Impedance control: An approach to manipulation," in *American Control Conference*, no. 21, 1984, pp. 304–313.

[25] ——, "Impedance control: an approach to manipulation. ii: Implementation," *Journal of dynamic systems, measurement, and control*, vol. 107, no. 1, pp. 8–16, 1985.

[26] B. Lukić, T. Petrič, L. Žlajpah, and K. Jovanović, "Kuka lwr robot cartesian stiffness control based on kinematic redundancy," in *International Conference on Robotics in Alpe-Adria Danube Region*. Springer, 2019, pp. 310–318.

[27] A. Q. Keemink, H. van der Kooij, and A. H. Stienen, "Admittance control for physical human–robot interaction," *The International Journal of Robotics Research*, vol. 37, no. 11, pp. 1421–1444, 2018. [Online]. Available: https://doi.org/10.1177/0278364918768950

[28] Y. Tao, T. Zhang, W. Xu, H.-Y. Tsang, J. Li, and Z. Wang, "A compact asymmetrical manipulator for robotic dentistry," in *2019 IEEE 9th Annual International Conference on CYBER Technology in Automation, Control, and Intelligent Systems (CYBER)*. IEEE, 2019, pp. 164–168.

[29] P. Puangmali, K. Althoefer, L. D. Seneviratne, D. Murphy, and P. Dasgupta, "State-of-the-art in force and tactile sensing for minimally invasive surgery," *IEEE Sensors Journal*, vol. 8, no. 4, pp. 371–381, 2008.